16th World Conference on Earthquake Engineering, 16WCEE 2017
Santiago Chile, January 9th to 13th 2017
Paper N° 4682
Registration Code: S-S1463098643

EXPERIMENTAL BEHAVIOR OF ELASTOMERIC BEARINGS AND SEISMIC BARS OF SIMPLY SUPPORTED CHILEAN BRIDGES

M. A. Hube[(1)], A. Martinez[(2)], F. Rubilar[(3)]

[(1)] *Associate Professor, Department of Structural and Geotechnical Engineering and National Research Center for Integrated Natural Disaster Management CONICYT/FONDAP/15110017, Pontificia Universidad Católica de Chile, mhube@ing.puc.cl*
[(2)] *Master of Science, Pontificia Universidad Católica de Chile, firubila@gmail.com*
[(3)] *Master of Science, Pontificia Universidad Católica de Chile, Antonio.benja.mg@gmail.com*

Abstract

Typical highway bridges in Chile consist on two span simply supported structures with prestressed concrete girders connected by a continuous slab. The girders are supported by elastomeric bearings which are not bolted and allow sliding of the superstructure. In some bridges, the lateral displacement of the superstructure is also restricted by lateral reinforced concrete or steel stoppers. According to the Chilean seismic design code, the bridges are designed with seismic bars, which are vertical steel rods that connect the superstructure with the bearing table and are intended to prevent the uplift of the superstructure. However, when bridges are subjected to large lateral displacements the seismic bars provide lateral restrain. The objective of this paper is to summarize the experimental campaigns of elastomeric bearings and seismic bars that were conducted at Pontificia Universidad Católica de Chile to characterize the seismic behavior of Chilean bridges. For the elastomeric bearings campaign, six bearings were tested under monotonic and cyclic loads. For the seismic bars campaign, five specimens were tested to quantify the lateral restrain that the seismic bars provide to the bridge superstructure. Two specimens represented the seismic bars of bridges with reinforced concrete diaphragm and three specimens represented those of bridges without diaphragm. From the conducted tests, the force deformation relationship of elastomeric bearings and seismic bars were obtained. Additionally, the behavior and failure mode of these elements were characterized.

Keywords: bridges, elastomeric bearings, sliding, reinforced concrete, experimental analysis

1. Introduction

Typical highway bridges in Chile consist on two span simply supported structures with prestressed concrete girders connected by a continuous reinforced concrete slab. The girders are supported by elastomeric bearings which are not bolted and allow sliding between the bearing and the heel of the beams, and between the bearing and the bearing table. The lateral displacement of the superstructure in some bridges is also restricted by lateral reinforced concrete or steel stoppers. According to the Chilean seismic design code [1], bridges are designed with seismic bars, which are vertical steel rods that connect the superstructure with the bearing table. These seismic bars are intended to prevent uplift of the superstructure and they are designed to resist certain vertical force. However, when the superstructure of a bridge is subjected to large lateral displacements, these seismic bars also provide lateral restrain. A typical overpass in Chile is shown in Fig. 1.

Fig. 1 – Typical Chilean overpass

Damage has been recently observed in Chilean bridges after 2010 Maule earthquake, and 2015 Illapel earthquake. Approximately 300 bridges were damaged, including 20 with collapsed spans, due to the Maule earthquake. Observed failure modes in this earthquake were: damage to connection between superstructure and substructure, unseating of spans in skewed and straight bridges do to transverse displacement and rotation of the superstructure, scour and pier damage due to tsunami action, among others [2]. More information of damaged bridges due to Maule earthquake is available elsewhere ([2], [3], [4] and [5]). After 2015 Illapel earthquake, minor damage was observed, and only eight bridges suffered damaged but without losing its functionality [6]. The observed damage was displacement of the superstructure due to sliding of elastomeric bearings, settlement of bridge approaches or damage to connection between superstructure and substructure. Examples of the observed damage in recent earthquakes are shown in Fig. 2. A collapsed bridge due to unseating of spans is shown in Fig. 2a). Permanent lateral displacement of the superstructure of Independencia overpass with damaged steel stoppers is shown in Fig. 2b). Las Mercedes underpass with significant lateral displacement is shown in Fig 2c). For such displacement, the seismic bars were expected to provide lateral restrain to the superstructure. Finally, Fig. 2d) shows sliding of elastomeric bearing in Talinay underpass after 2015 Illapel earthquake.

The objective of this paper is to summarize two experimental campaigns that were conducted at Pontificia Universidad Católica de Chile to characterize the seismic behavior of Chilean bridges. Two components of the bridge were tested under cyclic lateral loads: elastomeric bearings and seismic bars. Test of steel stoppers, as those observed in Fig. 2b), are summarized in Hube and Rubilar [7].

For the elastomeric bearings campaign, a total of six bearings were tested. Each bearing was subjected to four monotonic, and two cyclic loading protocols. The variables analyzed were the applied compressive stress, and the velocity of the applied lateral displacement. The bearings were supported by concrete blocks at the bottom and the top to simulate the contact with the heel of the girder and the bearing table, allowing the bearings

to slide. For the seismic bars campaign, five specimens were tested to quantify the lateral restrain that they provide to the bridge superstructure. Two specimens represented the seismic bars of bridges with reinforced concrete diaphragm, and three specimens represented those of bridges without diaphragm. From the conducted tests, the force deformation relationship of elastomeric bearings and seismic bars were obtained. Additionally, the behavior and failure mode of these elements were characterized.

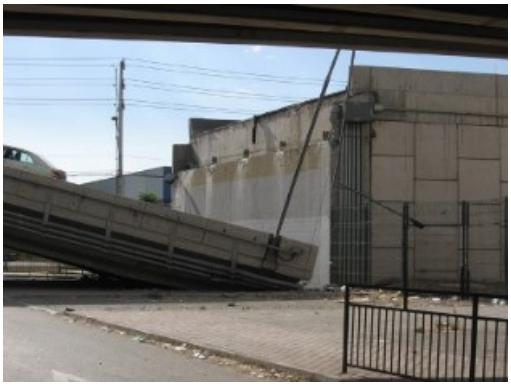

a) Unseating of span, Miraflores overpass, 2010 Maule Earthquake

b) Transverse displacement of superstructure, Independencia overpass, 2010 Maule earthquake

c) Transverse displacement of superstructure and deformed seismic bars, Las Mercedes underpass, 2010 Maule earthquake

d) Sliding of elastomeric bearing, Talinay underpass, 2015 Illapel earthquake

Fig. 2 – Observed damage in bridges after 2010 Maule, and 2015 Illapel earthquakes

2. Elastomeric Bearings

This section summarizes the experimental campaign conducted to characterize the seismic behavior of elastomeric bearings subjected to lateral loads. A total of six identical bearings (B1, B2, B3, B4, B5, and B6) were tested under monotonic and cyclic loads. The bearings dimensions were 400 x 500 x 90 mm and each bearing was reinforced with six steel plates. The thickness of the steel plates was 3 mm and the rubber height of each bearing was 72 mm. Detailed information of this test campaign is available elsewhere [8].

Each bearing was subjected to six loading cases, four monotonic, and four cyclic, as summarized in Table 1. The number in the load case in Table 1 is related to the compressive stress (in MPa) initially applied to the bearings. For the monotonic cases, the bearings were subjected to compressive stresses that varied from 1.0 MPa to 4.0 MPa. These values are within the range of 2.8 and 3.8 MPa identified by Rubilar [8] in a survey of Chilean bridges. For the cyclic tests, compressive stresses of 2 and 3 MPa were used for each bearing (Table 1). The bearings were subjected to increasing lateral displacements with three cycles at each amplitude. The

displacements amplitudes were 9, 22.5, 45, 90, 135, and 144 mm, which corresponded to shear deformations of 10, 25, 50, 100, 150, and 160%, respectively. The maximum target displacement of 160 mm was limited by the test setup. Additionally, for the cyclic tests, different bearings were subjected to different loading velocities to assess its effect on the seismic behavior. Cyclic tests C2 and C3 of bearings B1 and B2 were tested with a velocity of 25 mm/s. Cyclic tests C2 and C3 of bearings B3, B4, B5, and B6 were tested with a velocity of 10, 50, 75, and 100 mm/s, respectively.

Table 1 – Loading cases of each elastomeric bearing

Loading case	Loading type	Vertical load (kN)	Compressive stress (MPa)
M1	Monotonic	200	1.0
M2	Monotonic	400	2.0
M3	Monotonic	600	3.0
M4	Monotonic	800	4.0
C2	Cyclic	400	2.0
C3	Cyclic	600	3.0

2.1. Test Setup

The test setup of elastomeric bearings is shown in Fig. 3. The elastomeric bearings were placed between a top and bottom reinforced concrete blocks. The short side of the bearing (400 mm) was oriented in the direction of the applied load. The dimensions of the reinforced blocks were 1200 x1200 x100 mm and were constructed for these tests. The surface of the bottom reinforced concrete block was relatively rough to simulate the actual condition of the leveling mortar in cap beams under the bearings (Fig. 2d). The surface of the top reinforced concrete block was smooth, to simulate the surface of the bottom web of a prestressed reinforced concrete beam. This smooth surface was achieved by casting the block concrete on top of a wooden form. For the test setup, the smooth surface of the top concrete block was installed pointing down to simulate actual conditions.

The top and bottom reinforced concrete blocks were bolted to a steel loading frame that is used to test full-scale elastomeric bearings isolators at the laboratory of Pontificia Universidad Católica de Chile. The lateral load was applied with a 1,000 kN dynamic MTS actuator. The vertical load was applied to the bearings using five hydraulic jacks with a total loading capacity of 5,000 kN. The loads of these jack was transferred to the horizontal loading frame with a vertical steel frame, which can be observed in Fig. 3b).

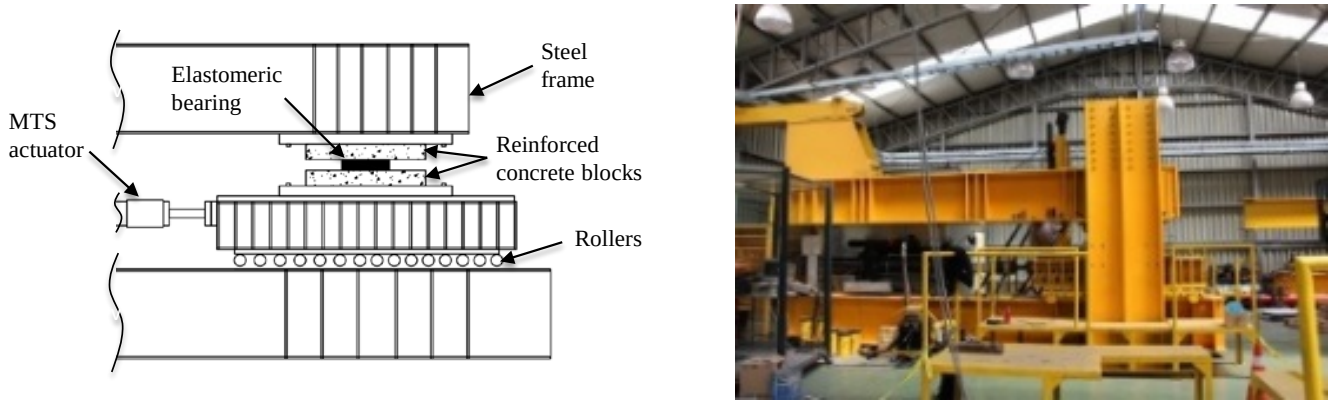

a) Drawing of the test setup b) Photograph of the test setup

Fig. 3 – Test setup, elastomeric bearings

2.2. Test Results

For the monotonic test, the lateral displacement was applied with a constant velocity of 2 mm/s. The bearings suffered shear deformation until sliding started to occur, as expected, at the contact of the bearings with the top reinforced concrete block. For the case of Talinay Bridge damaged after 2015 earthquake, sliding occurred between the bearing and the heels of the beam as observed in Fig. 2d). In such bridge, the coefficient of friction of the leveling mortar of the cap beam was smaller than that of the heel of the reinforced concrete beam. Fig. 4a) shows a deformed bearing when subjected to small lateral deformation and Fig. 4b) shows a bearing that is sliding at the top surface. The failure mode observed in all tests was sliding of the elastomeric bearing with respect to the top reinforced concrete block. The observed sliding failure mode is equivalent to that observed in the elastomeric bearings tested by Steelman et al. [9]. Delamination of internal shims, nor stability failure modes were observed in the tested bearings. Also, similar to the bearings tested by Steelman et al. [9], the structural integrity of the bearings was not compromised after the tests. Fig. 4c) shows the top worn surface of an elastomeric bearing after the six tests (Table 1) were the structural integrity is not compromised. Fig. 4d) shows the top reinforced concrete block after the tests with traces of rubber.

a) Bearing with lateral deformation

b) Bearing sliding

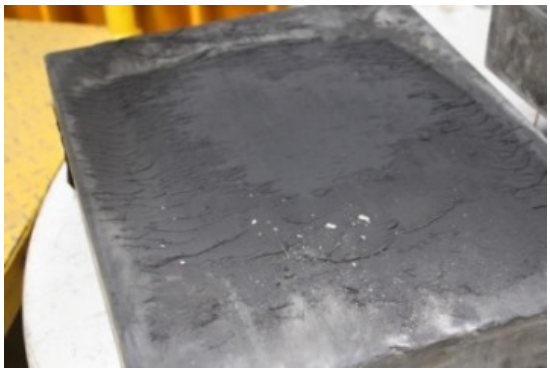

c) Surface of a bearing after the tests

d) Reinforced concrete block after the tests

Fig. 4 – Bearing tests photographs

The load displacement relationships obtained for the monotonic tests of bearings B1 and B2 are shown in Fig 5. A linear behavior is identified until the peak load is achieved, except for test B2-M1 in Fig. 5b, were a change of stiffness is observed at about 35 mm displacement. At the peak load, the static coefficient of friction was reached, and the bearings started to slide with respect to the top reinforced concrete block. For larger displacements, a relatively constant load was measured in all bearings, which magnitude is related to the coefficient of kinetic friction. The maximum strengths (F_{max}) measured in the four monotonic tests conducted to each of the six bearings are summarized in Table 2. Additionally, the table contains the measured static coefficient of friction (μ_s) for each case.

For compressive stresses larger 1.0 MPa (load cases M2, M3 and M4), Table 2 shows that the average maximum strengths are relatively constant. This is caused by the decrease of the static coefficient of friction with the increase of compressive stress. An average coefficient of friction of 0.58 was measured for monotonic tests M1 with compressive stress of 1.0 MPa, and 0.24 for monotonic tests M4 with compressive stress of 4.0 MPa (Table 2).

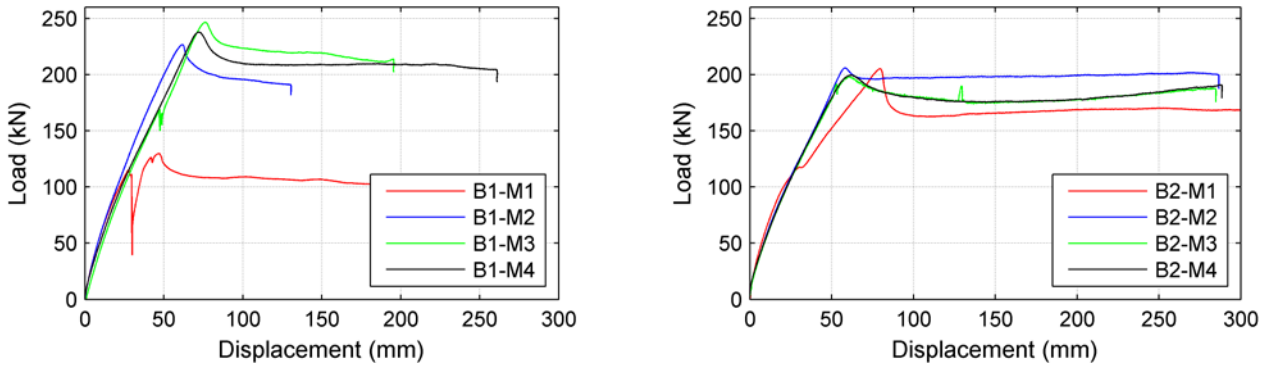

a) B1 b) B2

Fig. 5 – Load displacement relationships, monotonic tests, bearings B1 and B2

Table 2 – Maximum strength (F_{max}) and static coefficient of friction (μ_s), monotonic tests of elastomeric bearings

Bearing	F_{max} (kN)				μ_s			
	M1	M2	M3	M4	M1	M2	M3	M4
1	129.7	226.7	246.5	237.7	0.65	0.57	0.41	0.30
2	205.2	205.9	198.4	199.5	1.03	0.52	0.33	0.25
3	115.6	223.1	205.0	201.3	0.58	0.56	0.34	0.25
4	86.1	166.3	199.6	168.0	0.43	0.42	0.33	0.21
5	80.0	171.8	154.4	163.6	0.40	0.43	0.26	0.21
6	82.8	165.7	163.7	174.3	0.41	0.41	0.27	0.22
Average	116.6	193.3	194.6	190.7	0.58	0.49	0.32	0.24

The load displacement relationships obtained for the cyclic tests of bearings B1 and B4 are shown in Fig 5. Bearing B1 was tested with a velocity of 25 mm/s and bearing B4 with a velocity of 50 mm/s. For small displacements cycles, the bearings performed relatively elastically and some energy dissipation is observed. The maximum strength in most tests was achieved at the displacement cycles of 90 mm (100% shear deformation). For larger displacements, the strength was reduced and sliding occurred in both directions. The maximum strengths (F_{max}) and the static coefficient of friction (μ_s) measured in the cyclic tests conducted to each bearings are summarized in Table 3. Equivalent to the results of the monotonic tests, the measured coefficient of friction for bearings tested with a compressive stress of 3 MPa were smaller than those tested with a compressive stress of 2 MPa. Regarding the velocity of testing, no clear trend was observed.

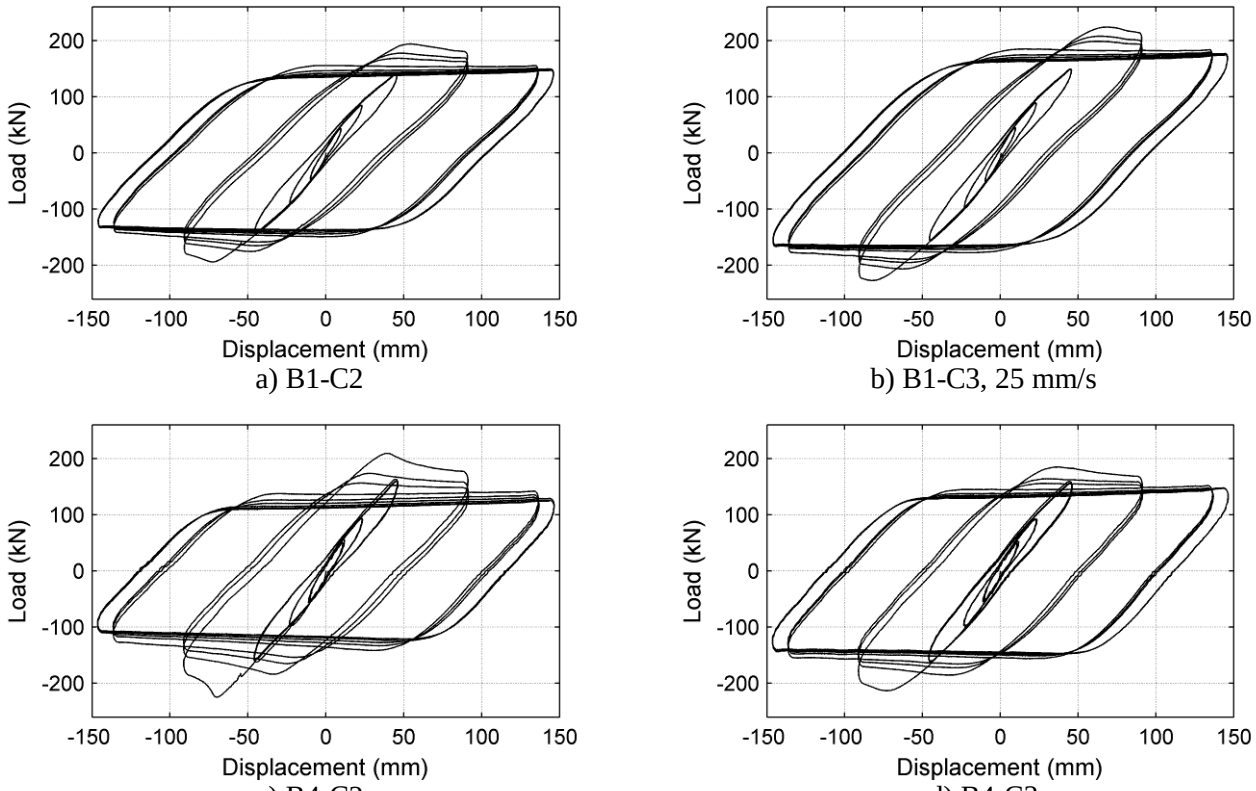

a) B1-C2 b) B1-C3, 25 mm/s

c) B4-C2 d) B4-C3

Fig. 6 – Load displacement relationships, cyclic tests bearings B1 and B4, tested with loading velocity of 25 mm/s and 50 mm/s respectively

Table 3 – Maximum strength (F_{max}) and static coefficient of friction(μ_s), cyclic tests of elastomeric bearings

Bearing	Velocity (mm/s)	F_{max} (kN)		μ_s	
		C2	C3	C2	C3
1	25	193.9	0.49	223.9	0.37
2	25	161.2	0.40	172.4	0.29
3	10	179.6	0.45	165.0	0.27
4	50	209.3	0.52	185.0	0.31
5	75	180.3	0.45	193.3	0.32
6	100	226.2	0.57	196.4	0.33

3. Seismic Bars

This section summarizes the experimental campaign conducted to characterize the seismic behavior of the seismic bars of bridges when subjected to lateral displacements of the superstructure. Two specimens were tested to simulate the behavior of seismic bars of bridges with diaphragms (WD), and three to simulate the behavior of bridges without diaphragms (WOD). The seismic bar specimens were subjected to cyclic lateral displacements and the test matrix is summarized in Table 4, where the clear distance of the seismic bar is the distance between the top of the bearing table and the bottom of the slab or reinforced concrete diaphragm, as shown below. The

characteristics of the seismic bars of Chilean bridges were obtained from a survey of 13 bridges [10]. Two seismic bars are typically installed between prestressed concrete girders at each side of the span, as observed in Fig. 2c). The average diameter of these bars is 22 mm and the specified yield strength of the steel is usually 280 MPa.

Table 4 – Test matrix, seismic bars

Specimen	Loading direction	Clear distance h_l (mm)
WD1	Both directions	100
WD2	Both directions	100
WOD1	Both directions	720
WOD2	Both directions	720
WOD3	One direction	720

3.1. Test Setup

The proposed seismic bars specimens represent a portion of the bridge with two seismic bars between a pair of consecutive girders. Each specimen consist on a bottom reinforced concrete block representing the bearing table of the substructure, and a top reinforced concrete wall or beam representing the reinforced concrete diaphragm or slab, depending on the case. Additionally, each specimen comprised two vertical seismic bars connecting the bottom and top reinforced concrete blocks. The specimens were constructed using ½-scale with and the diameter of the seismic bars was 16 mm. Fig. 7 shows the test regions of a bridge and the constructed specimens for cases WD and WOD. The clear distance of the seismic bars h_l (refer to Fig. 8) was 100 mm and 720 mm for specimens WD and WOD, respectively. Fig. 8 shows pictures of the test setup for both cases. More information of these tests is available elsewhere [12].

The seismic bars were anchored in the bottom reinforced concrete block with 90-degree hooks and the development length was estimated following ACI [11] recommendations. At the top edge of the seismic bars a 90 mm long thread was manufactured. This thread was used to bolt the seismic bars to the top diaphragm or slab using a washer and two nuts, following construction practices. Since a prestressed force is not required according to the bridge design code [1], they were bolted manually with a regular wrench. The slab and diaphragms were constructed with two cylindrical vertical perforations to allow the seismic bars to pass through them. To simulate construction practice, PVC tubes of 60 mm outside diameter and 3 mm thickness were embedded in the slab and diaphragm to achieve these perforations. For the seismic bars, A440-280H steel was used with nominal yield strength of 280 MPa.

The lateral load was applied with an actuator with a capacity of 610 kN in compression and 340 kN in tension. The actuator was bolted to the reinforced concrete slab or diaphragms of the specimens using two steel plates. The bottom reinforced concrete block was attached to the strong floor with two transverse steel beams that were bolted to the strong floor. For both type of specimens, the vertical displacement of the diaphragm or slab was restricted with two rollers at the top and two rollers at the bottom. The bottom rollers simulate the vertical restraint provided by the elastomeric bearings, and the top rollers prevented the uplift of the diaphragm or slab. In real bridges, the uplift of the superstructure is prevented by its own weight. For the specimens WOD, the reinforced concrete slab was placed on top of two parallel steel beams to provide additional flexural stiffness and strength to the slab, but allowed the free displacement of the seismic bars between them.

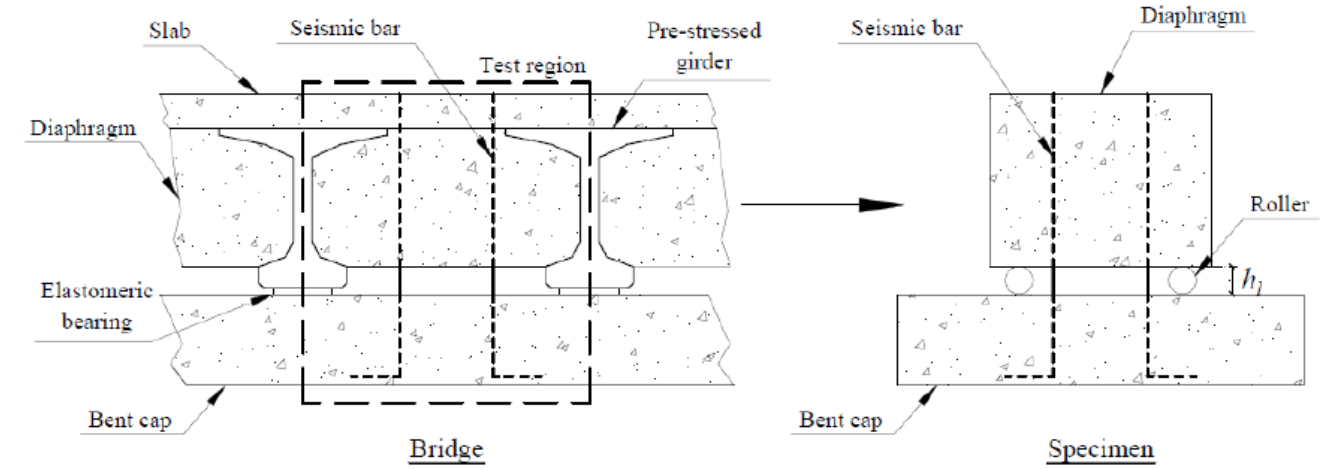

a) Specimens with diaphragms

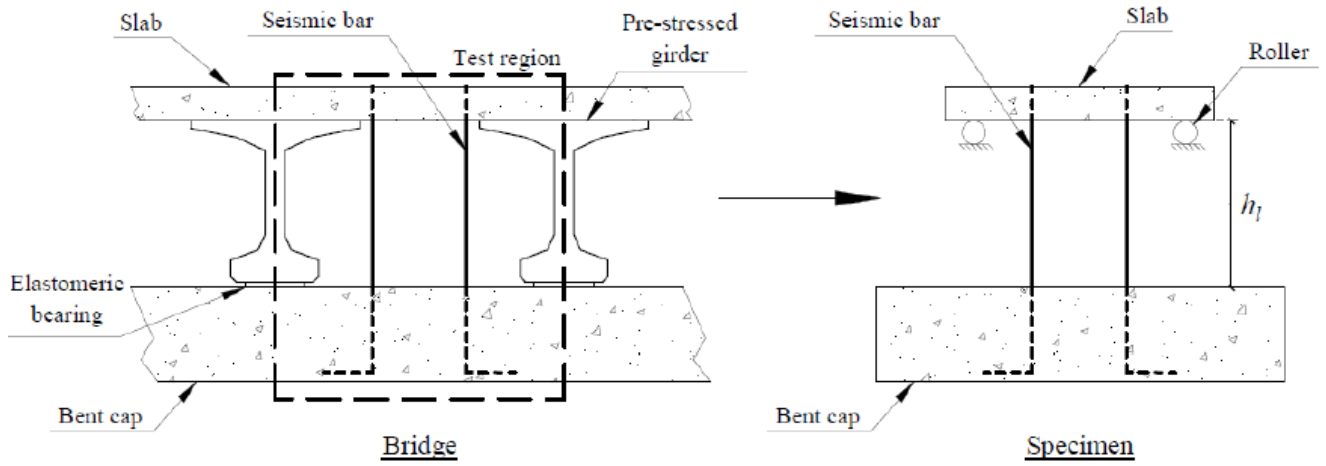

b) Specimens without diaphragms

Fig. 7 – Definition of seismic bar specimens

a) Specimens with diaphragms

b) Specimens without diaphragms

Fig. 8 – Test setup, seismic bars

3.2. Test Results

Before applying the horizontal displacement, the seismic bars were prestressed manually using a regular wrench. The initial prestress was totally or partially lost after a few cycles, before reaching the yield point of the bars, probably due to localized yielding of the threads of the seismic bars.

For the specimens WD, which were characterized by a clear distance of 100 mm, contact of the seismic bars with the embedded PVC tubes of the diaphragm was first observed at the cycle with displacement amplitude of 20 mm. This instant is shown in Fig. 9a) for specimen WD2. For cycles with displacement amplitude larger than 50 mm, the nuts of the seismic bars lifted when the specimens were passing through zero displacement, as can be observed for specimen WD2 in Fig 9b). Both specimens WD failed due to fracture of the seismic bars at the beginning of the first cycle with displacement amplitude of 150 mm, and were not able to reach such displacement amplitude. The fracture of the seismic bars occurred at the contact with the bent cap, possibly due to stress concentration and fatigue experienced by the seismic bars. The forces generated by the contact between the seismic bars and the PVC tubes in the diaphragm caused damage to the PVC and concrete at the bottom of the diaphragm.

a) Seismic bars touching the PVC tuves of the diaphragm, specimen WD2

a) Uplift of the seismic bar nuts, specimen WD2

Fig. 9 – Seismic bars photographs

For the specimens WOD it was not possible to observe the exact moment in which the seismic bars touched the PVC tubes embedded in the slabs because of the presence of the steel beams of the test setup (Fig. 8b). For cycles with displacement amplitude larger than 144 mm, the nuts of the seismic bars lifted, implying that the prestress force of the seismic bars was lost. The failure of the specimens WO1 and WOD2 was not achieved at the end cycles, where the largest amplitude of 190 mm was restricted by the actuator stroke. Therefore, specimen WOD3 was loaded only with positive displacement to achieve larger displacements. The failure of specimen WOD3 occurred during a cycle with displacement amplitude of 320 mm. The failure mode of specimen WOD was fracture of both seismic bars at the threads location above the slab. The north bar fracture 15 seconds earlier than the south bar. Finally, the damage observed in the concrete of the slab of specimens WOD was less than that on the diaphragms of specimens WD. This reduced damage is explained by the larger clear distance of seismic bars in specimens WOD.

The load-displacement relationships of the seismic bars specimens with diaphragms and specimens WOD1 and WOD2 without diaphragms are shown in Fig. 9 and 10, respectively. The shown lateral force corresponds to the actuator measured forces minus friction forces generated in the rollers due to

the test setup. These friction forces were measured in cycles after the fracture of the seismic bars. For specimens WD the average maximum lateral load was 85 kN at an average displacement of 97 mm. For the specimens WOD and average maximum lateral load of 32.5 kN was measured in WOD1 and WOD. However, failure occurred in WOD3 at an average load of 66.4 kN. This failure occurred at a displacement of 272 mm. From the results of Fig. 8 and Fig. 9 it can be observed that the lateral restrain provided by seismic bars in bridges with diaphragm is larger than that in bridges without diaphragm. Additionally, both figures shown that the unloading stiffness is steep, implying that the restitution lateral force is quickly lost when the superstructure is returning to the center.

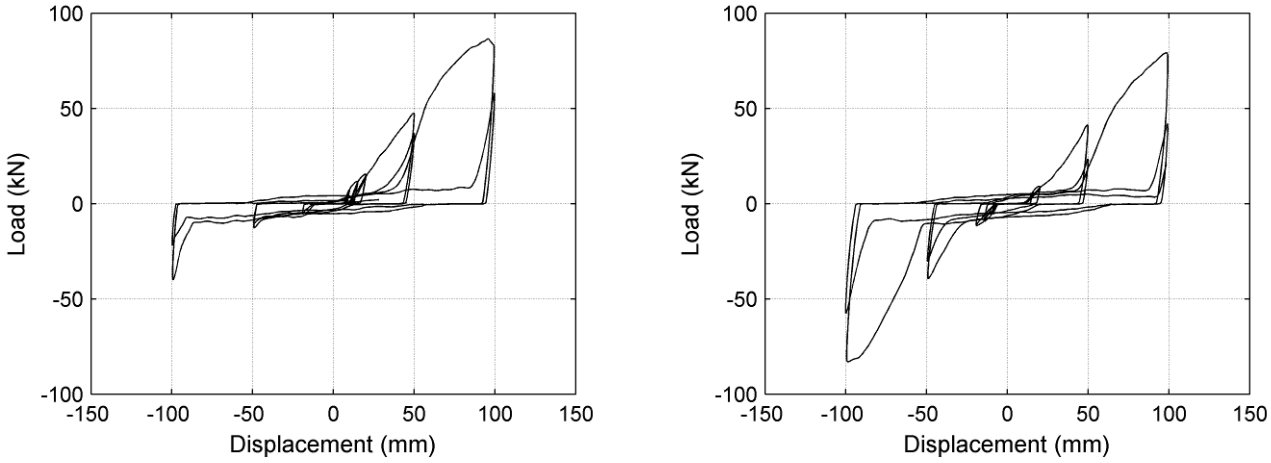

a) WD1 b) WD2

Fig. 9 – Force displacement relationship, seismic bars with transverse diaphragms

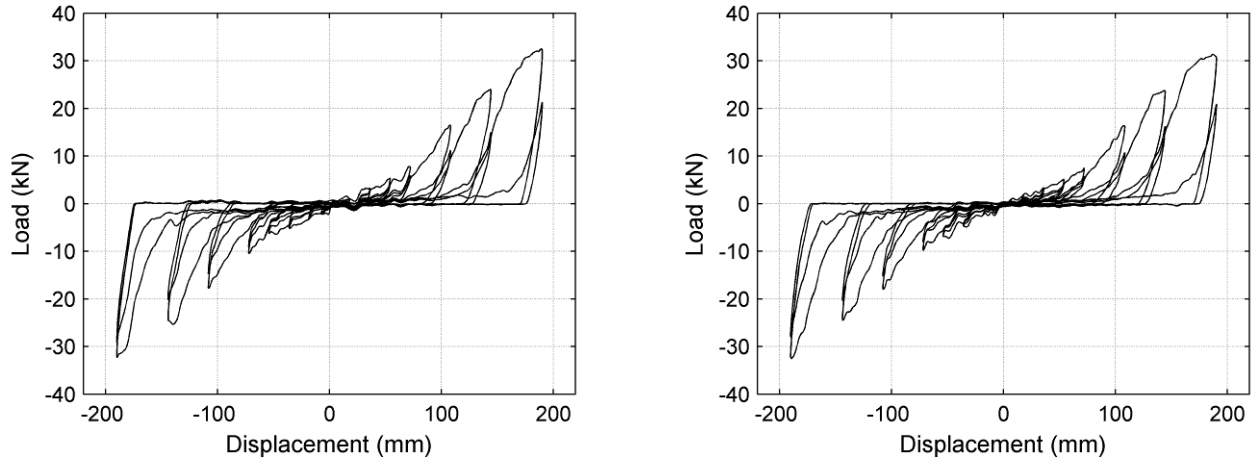

a) WOD1 b) WOD2

Fig. 10 – Force displacement relationship, seismic bars without transverse diaphragms

4. Conclusions

The objective of this paper is to summarize the experimental campaigns of elastomeric bearings and seismic bars that were conducted at Pontificia Universidad Católica de Chile to characterize the seismic behavior of Chilean bridges. For the elastomeric bearings campaign, six bearings were tested under monotonic and cyclic loads. The variables analyzed were the applied compressive stress, and the velocity of the applied lateral displacements. For

the seismic bars campaign, five specimens were tested to quantify the lateral restrain that they provide to the bridge superstructure

From the test of the elastomeric bearings, it was concluded that the coefficient of friction decreases as the compressive stress of the bearing increases. From the test of the seismic bars, it was concluded that these bars are more effective in bridges with diaphragm than in bridges without diaphragm. Additionally, the vertical restrain provided by these bars is not effective under cyclic behavior because the prestress of the bars is lost under cyclic displacements. The obtained results may be used to calibrate numerical models for seismic risk assessment of existing or new bridges.

5. Acknowledgements

This study has been sponsored by the National Research Center for Integrated Natural Disaster Management CONICYT/FONDAP/15110017 (CIGIDEN). Both tests were funded by Fondecyt through grant 11121581. The authors also acknowledge Camilo Guzman and Nicolas Tapia from the Structural Engineering Laboratory of Pontificia Universidad Católica de Chile.

7. References

[1] Ministerio de Obras Públicas (2015): Highway manual, instructions and design criteria, (in Spanish).

[2] Buckle I, Hube M, Chen G, Yen W, Arias J (2012): Structural performance of bridges in the offshore Maule earthquake of February 27 2010. *Earthquake Spectra*, **28** (S1), S533-S552.

[3] Schanack F, Valdebenito G, Alvial J (2012): Seismic damage to bridges during the 27 February 2010 magnitude 8.8 Chile earthquake. *Earthquake Spectra*, **28** (1) 301-315.

[4] Kawashima K, Unjoh S, Hoshikuma,JI, Kosa K (2011): Damage of Bridges due to the 2010 Maule, Chile, Earthquake. Journal of Earthquake Engineering, **15** (7), 1036-1068.

[5] Toro F, Rubilar F, Hube MA, Santa-María H (2013): Critical variables that affected the seismic behavior of Chilean underpasses during 2010 Maule Earthquake. *7th National Seismic Conference on Bridges & Highways*, Oakland, USA

[6] Rivera F, Jünemann R, Candia G, Favier F. Fernández C, Chacón M, Hube M, Chamorro A, Aguirre P, de la Llera JC, Poulus A (2016). Reconnaisanc observations by CIGIDEN after the 2015 Illapel, Chile earthquake and tsunami. *16th World Conference on Earthquake Engineering*, Santiago, Chile.

[7] Hube MA, Rubilar F (2012): Capacity evaluation of steel stoppers of reinforced concrete Chilean bridges. *The International Symposium for CISMID 25th Anniversary*, Lima, Peru.

[8] Rubilar F (2014): Nonlinear model to predict the seismic responses of overpasses. *Master of Science Thesis*, Pontificia Universidad Católica de Chile, Chile (in Spanish).

[9] Steelman J, Fahnestock LA, Filipov EV, LaFave JM, Hajjar JF, Foutch DA (2013): Shear and friction response of nonseismic laminated elastomeric bridge bearings subject to seismic demands. *Journal of Bridge Engineering*, **18** (7) 612-623.

[10] Martinez A (2015): Effect of the seismic bars in the transverse seismic behavior of reinforced concrete bridges. *Master of Science Thesis*, Pontificia Universidad Católica de Chile, Chile (in Spanish).

[11] American Concrete Institute (2014): Building code requirements for structural concrete and commentary, ACI 318-11, Farmington Hills, MI.

[12] Martínez A, Hube MA, Rollins KM (2016): Analytical fragility curves for highway bridges in Chile. Under Review, *Engineering Structures.*